

Relations of pulsatility index and particle residence time to the wall-shear-stress properties in pulsating flows with reverse flow phase

Dikla Kersh* · Alex Liberzon

Received: date / Accepted: date

Abstract Pulsating flows with a *total reverse flow* phase are ubiquitous in physiological systems in normal and pathological conditions. Irregularity of hemodynamic parameters in such flows is correlated with the appearance and development of several arterial pathologies. We study the relations between flow waveform parameters and the wall shear stress (WSS) related quantities such as mean, root-mean-square, gradient of WSS and the oscillating shear index. The phase-averaged velocity profiles measured by the digital particle image velocimetry are used to estimate WSS utilizing the Womersley pulsating flow model. In addition to the Reynolds and Womersley numbers, another dimensionless parameter, pulsating index (PI) which is the ratio of forward flow rate to the reverse flow rate is required. PI is essential for the complete description of the flow patterns with the

D. Kersh · Alex Liberzon

School of Mechanical Engineering

Tel Aviv University, Tel Aviv 69978, Israel

E-mail: diklakersh@gmail.com

total flow reversal. We demonstrate significant effects on the WSS quantities due to the pulsating frequency and PI. Furthermore, the particle residence time (PRT), measured using the three-dimensional particle tracking velocimetry, shows significant correlation with WSS related quantities. For example, shorter residence time correlates strongly with the high pulsatility index. Correlations of other quantities are qualitatively similar though weaker, suggesting cross-coupling effects. It is proposed that PRT, estimated in-vivo from the trajectories of magnetic or contrast tracers, can provide an alternative diagnostics of wall shear stress parameters.

Keywords reverse phase · retrograde flow · pulsatile flow · wall shear stress · particle residence time · digital particle image velocimetry · three-dimensional particle tracking velocimetry

1 Introduction

Flow patterns with a *total reverse phase*, i.e. a phase with a negative flow rate typically referred to as retrograde or regurgitate flows, are present in the cardiovascular system. During flow reversal, the fluid flow direction is altered and the velocity gradients change sign abruptly. *Local flow reversal* occurs when the fluid in the near wall region is reversed, while the total flow rate of the cross section is positive. Aorta flow experiences a total reverse phase that results from the rapid deceleration of blood at the end of systole before the closing of the aortic valve [6, 13, 15]. Increase in the amplitude or duration of the reverse flow phase is associated with rapid blood flow elevation which can result from invasive procedure or arterial pathology [4, 12]. Haddad et al. [7] predicted a different form of local flow reversal, the so called “off wall reversal”, where the negative velocity is found at a

certain distance from the wall, while the near wall velocity is positive. One of the main interests in pulsating flows with the total reverse phase is the shear stresses developed on the arterial wall. Arterial wall shear stresses (WSS) are known as a main regulator of endothelial cell function and vascular structure [4, 14]. Irregular values of WSS properties are strongly related to cardiovascular pathologies. Despite the clinical importance, a detailed analysis of the important hemodynamics parameters, along with the reliable measurements of WSS in flows with the total reverse phase, is lacking. Although a variety of non intrusive imaging based measurements such as MRI, Ultrasound and particle velocimetry are available, accurate measurement very close to the wall are non-trivial to obtain due to the limited spatial resolution, light reflections and deficit of tracer particles in the area. Due to the high uncertainty in the near wall region data, the curve-fitting or model-fitting approaches are commonly used [10].

Pulsating cardiovascular flows with local flow reverse are well described using two dimensionless parameters: the Reynolds and the Womersley numbers. For example, Finol et al. [3] found that the maximal values of non-dimensional mean wall shear stress and non-dimensional wall shear stress gradient increase with the Reynolds number, while Ref. [8] demonstrated the significant effect on WSS magnitude of the Womersley number. We show that in case of the pulsating flows with the total reverse phase, a complete description of the flow is not possible without an additional dimensionless parameter, the pulsatility index (PI), [5]. This index is an arterial blood-flow velocity parameter quantifying the pulsatility or oscillations of the flow waveform, e.g. [17].

We estimate the wall shear stress τ , its root-mean-square (τ_{mag}), time gradient (WSSG), and oscillating shear index (OSI), using digital particle image velocime-

try (DPIV), and reveal their dimensionless relations. In addition, we measure Lagrangian trajectories of flow tracers using the three-dimensional particle tracking velocimetry (3D-PTV) and demonstrate insightful correlations between the directly estimated particle residence time (PRT) and WSS for different flow conditions. In regions of recirculation (regions of increased plague deposits), particles have significantly longer times of residence and therefore this parameter was correlated with hemodynamic properties in flows with a *total reverse phase*.

2 Materials and Methods

2.1 Experimental method

A custom-design flow test rig was developed to create well-controlled pulsatile flows, as shown in Fig. 1.

[Fig. 1 about here.]

The pulsating flow is created in an elastic tube (made of Tygon B-44-4X, Saint Gobain, inner diameter of 3/4" and wall thickness of 1/8", $L/d \geq 40$, elasticity modulus of 12 MPa, estimated distensibility $1.36 \times 10^{-6} \text{ Pa}^{-1}$) by a set of three DC voltage driven computer controlled gear pumps. In order to allow high quality optical measurements, the tube was placed in a $800 \times 300 \times 200$ mm glass tank filled with a refractive index matched liquid (60%_w glycerin-water solution). A 40%_w glycerin-water solution was used as blood mimicking fluid. The flow was monitored using pressure transducers (EW-68075-02, Cole Parmer) and magnetic flow meter (MAG 1100, Danfoss). We created a set of flow waveforms (dipolar and unipolar sine w/o total flow reversals, unipolar sine, cardiovascular-like waveform,

see Fig. 2) in the following range of the flow parameters: Reynolds number between $60 \div 900$, Womersley number $\alpha : 6 \div 11$ and pulsatility index (PI) $1.5 \div 9$.

[Fig. 2 about here.]

We implemented DPIV using a dual Nd:YAG laser (532 nm, 120 mJ/pulse, Solo 120XT, New Wave Research), a high-resolution CCD camera (12 bit, 4008×2672 pixels, TSI Inc.) as shown in Fig. 3a. Silver-coated hollow glass spheres ($14 \mu\text{m}$, 1.05 g/cm^3 , TSI Inc.) were used as seeding particles. More than 100 images were acquired at each of the 7 phases of the pulse period, triggered by the pressure transducer. Phase averaged velocity was estimated using a commercial software (Insight 9.1, TSI Inc.) and verified with an open source software [16] (www.openpiv.net).

Lagrangian trajectories of fluorescent microspheres (nominal diameter $60 \mu\text{m}$, $\rho = 1.51 \text{ g/cm}^3$) were measured using 3D-PTV, as presented in Fig. 3b, illuminated by the LED light source (*MB – LL306 – R – 24*, MetaPhase Tech.) and recorded using 4 high-speed cameras (8 bit, 1280×1024 pixels, Mikrottron GmbH) and stored on the digital video recording system (IO Industries) at rates of $100 \div 250$ fps. Open source software (www.openptv.net) is used for image processing [11]. Detailed description of the experimental method is given in [9,6].

[Fig. 3 about here.]

[Table 1 about here.]

2.2 Wall shear stress related properties

Wall shear stresses were estimated using two methods: a) by derivation of measured near wall velocity using 3 points curve fitting, and b) by utilizing the Womersley

solution for pulsating flow in a rigid tube [19]. The flow rate waveform Q has been calculated by integrating the measured velocity profiles. The Fourier coefficients of the signal were calculated using fast Fourier transform ($k = 32, N = 100$):

$$Q_k = \sum_{n=0}^{N-1} Q_n e^{-j \frac{2\pi k n}{N}}, \quad (1)$$

where Q_n is the n^{th} component of the flow rate waveform in its Fourier representation. Velocity profiles are estimated from the Fourier representation of the flow rate waveform according to the inverse Womersley relations:

$$u(r, t) = Re \left\{ \sum_{n=0}^N \frac{Q_n}{\pi R^2} \left(\frac{j^{3/2} \alpha_n J_0(j^{3/2} \alpha_n) - j^{3/2} \alpha_n J_0(j^{3/2} \alpha_n r/R)}{j^{3/2} \alpha_n J_0(j^{3/2} \alpha_n) - 2J_1(j^{3/2} \alpha_n)} \right) e^{j\omega n t} \right\} \quad (2)$$

where J_0, J_1 are the zero and first order Bessel functions respectively, ω is the pulsation frequency, $j = \sqrt{-1}$ and α_n is the n^{th} Womersley number defined as $\alpha_n = R\sqrt{\frac{\omega n}{\nu}}$ and R is the inner radius of the pipe. Finally, WSS can be estimated deriving the obtained Womersley velocity profiles at different phases.

The flow waveforms were characterized using three dimensional numbers: the maximal velocity Reynolds number Re_{max} :

$$Re = Re_{max} = U_{max} D / \nu, \quad (3)$$

where U_{max} is the maximal time averaged velocity, D is the tube inner diameter and ν is the kinematic viscosity of the fluid; the Womersley number α :

$$\alpha = R\sqrt{\omega/\nu} \quad (4)$$

and the pulsation index (PI):

$$PI = (Q_{max} - Q_{min}) / Q_{mean} \quad (5)$$

Flow waveforms with *total reverse flow* phases are characterized by high PI values. The following WSS related properties are considered in the present study:

dimensionless mean wall shear stress, τ_{mean}^* :

$$\tau_{mean}^* = \frac{1}{\tau_s} \left(\frac{1}{T} \int_0^T \tau(R, t) dt \right) \quad (6)$$

Hereinafter the superscript * denotes the dimensionless parameters, normalized using the time period of the pulsation, T , and the equivalent Poiseuille wall shear stress τ_s :

$$\tau_s = \frac{16\mu\bar{U}}{R}, \quad (7)$$

where \bar{U} is the mean value of the time averaged velocity profile in the cross section, $\bar{U} = Q_{mean}/\pi R^2$. Another hemodynamic parameters is the wall shear stresses magnitude, averaged over a cycle:

$$\tau_{mag}^* = \frac{1}{\tau_s} \left(\frac{1}{T} \int_0^T |\tau(R, t)| dt \right), \quad (8)$$

where $|\cdot|$ denotes the absolute values of the WSS $\tau(R, t)$. Next are the oscillatory shear index (OSI):

$$OSI = \frac{1}{2} \left(1 - \frac{\tau_{mean}^*}{\tau_{mag}^*} \right) \quad (9)$$

and the time averaged wall shear stresses gradient (WSSG):

$$\overline{WSSG}^* = \frac{1}{\tau_s} \frac{1}{T} \left(\frac{1}{T} \int_0^T \left| \frac{\partial \tau(R, t)}{\partial t} \right| dt \right) \quad (10)$$

In addition to the measurements, we analyze the same properties for a larger variation of the dimensionless parameters Re, α, PI , using a simulation based on the Womersley solution, namely $Re = (70, 170, 200, 350, 690)$; $\alpha = (6, 8, 9, 11, 13)$; $PI = (1.5, 2.5, 4, 5, 6.5, 9)$. In each simulation run, only one parameter was changed while the other two were kept constant. Experimentally obtained WSS and related

quantities are compared in the following to the trends of these hemodynamic parameters estimated from the simulation.

3D-PTV experimental method provides the velocity and accelerations of Lagrangian tracers in the region of interest and during the time of pulsation. Moreover, we deduce from the Lagrangian dataset the particle residence time (PRT), defined here as the time interval required for a particle to exit a spherical domain of pre-defined radius r_o :

$$\text{PRT}(x_0, t, r_o) = t : |\underline{x}(t) - \underline{x}(t_0)| > r_o \quad , \underline{x} = (\underline{r}, t) \quad (11)$$

We estimate PRT for a number of values in the range of $r_o = 0 \div 0.25$ mm, averaging PRT values of all measured trajectories in a given experimental run, and present in the following a comparative study of the flow patterns.

3 Results

3.1 Velocity profiles

DPIV measured velocity profiles (symbols) and their corresponding Womersley solutions (curves), according to Eq.(2), are presented in figure 4 for 16 different runs and different phases, θ . Profiles at the beginning of the cycle and at the acceleration phases are rectangular in shape, as described in the literature for mid frequency laminar flows [19, 18]. Near wall local flow reversal can be seen in most runs for $\theta > 180^\circ$. *Total flow reversal* appeared in runs 11, 14, 16. It can be seen that on overall, the measured velocity profiles fit well with the Womersley solution. On average, the deviation of the measured velocity values from the analytical solution is below 18%. As it can be expected, the strongest deviations are found in the

near-wall region. WSS estimated from measured velocity profiles shows a good compatibility to WSS calculated from the inverse Womersley solution within the average uncertainty limits of 20%.

[Fig. 4 about here.]

3.2 Dimensional analysis of WSS properties

Comparison between simulated WSS values and quantities calculated from measurements can be seen in figure 5. Dimensionless WSS related quantities are not influenced by the variation of Reynolds number if the Womersley number and pulsatility index are kept constant (not shown here). Mean WSS (τ_{mean}), according to the Womersley model, is constant and equal to $0.75\tau_s$ (dashed line in Fig. 5a). Normalized WSS magnitude, shown in Fig. 5b, maintains a constant value for $\text{PI} = 1.5$. For higher PI values, WSS magnitude increases with an increase in PI or frequency, when the effect of increasing PI is more significant. Oscillating shear index (OSI) is shown in Fig. 5c. Minimal values are received for the lowest pulsatility index tested, i.e. $\text{PI} = 1.5$ and are frequency dependent. OSI values increases substantially for the range of $1.5 < \text{PI} < 6$, showing dependency of both PI and the Womersley number. For $\text{PI} > 6$, the OSI values increased rate is reduced and apparently saturates to an asymptotic value. WSSG maintains a quasi-constant value and it does not dependent on PI for the lowest range of Womersley numbers tested, (Fig. 5d). However, for the higher frequencies, WSSG values increase almost linearly with both frequency and PI. Measured WSS magnitude and WSSG usually follows the simulation trend, except for runs with *substantial reverse flow*

phase, where the discrepancies can not be explained by the measurement uncertainty. OSI values shows grater discrepancies compared to other quantities.

[Fig. 5 about here.]

3.3 Particle residence time

Mean particle residence time, estimated according to Eq.(11), as a function of the sphere radius r_0 is presented in figure 6. It can be seen that particle residence time increases with r_0 , as expected, though at different rates. Comparing the residence time of two runs at the same Reynolds number, we observe shorter residence time for higher PI. The same trend is observed when we compare the runs at the same frequency - the residence time is shorter for higher PI. According to the analysis above, WSS related quantities are strongly influenced by pulsatility index (PI). This fact indicates a possible relation between the particle residence time and WSS related properties.

[Fig. 6 about here.]

In order to test this hypothesis, we plot the PI, OSI and WSSG versus PRT for all the runs in Fig. 7a-c at constant r_0 ($200\ \mu m$). The results show very strong correlation between particle residence time and pulsatility index. Thus, runs with shorter residence time are characterized by higher PI values. The correlation between the particle residence time and OSI or WSSG is not as good, nevertheless, the general trend is clearly seen - the particles residence time is short when the OSI and WSSG are high.

[Fig. 7 about here.]

4 Summary and discussion

DPIV measured velocity profiles show good agreement with the Womersley's analytical solution for pulsating flow in rigid tubes, with slight deviations of the measurements from the analytical solution near the wall. We can address the deviations to the relatively lower quality of measured data due to light reflections and inherent inaccuracy of defining the wall location in DPIV images. Thus comparing measured data to model profiles and applying image processing methods, the closest distance from the wall, for which PIV velocity measurement can be considered as reliable, is estimated as 0.7 mm or $0.07y/R$. Therefore, the Womersley rigid tube flow model can be considered a suitable reference for measured flow properties.

Using computational simulations based on the Womersley solution and the experimental results, we show that properly normalized WSS properties do not depend on the Reynolds number at the same frequency of pulsations. However, different values of WSS related properties were found for flows with an equal Reynolds number and Womersley number but for different waveforms. We conclude that the two parameters are not sufficient to describe all the relevant flow properties and an additional parameter is introduced, namely the pulsatility index (PI), calculated from the properties of the flow rate waveform [10]. Experimental runs with *total flow reversal* phase are characterized by *high PI values*. Simulations based on the Womersley model show that the WSS related quantities (except the mean normalized τ_{mean}^*), are highly influenced by the two parameters: PI and the Womersley number. WSS magnitude and WSSG both increase with increase of PI/frequency. PI is stronger correlated with the WSS magnitude, while the Wom-

ersley number affects stronger the WSSG. WSS magnitude and WSSG follow the trends obtained from the simulations, except for the experimental runs with *total flow reversal*. Measured OSI values are significantly lower than predicted values. OSI values may be influenced by the *duration of the reverse flow phase* - parameter that was not considered in the present study.

Since direct WSS measurements in *in-vitro* and *in-vivo* applications are difficult, the indirect non-intrusive methods, such as particle residence time (PRT) can become valuable measures of the local WSS related properties. PRT can be measured by the 3D-PTV method in flows with local or total flow reversal as the time required for a particle to exit the near wall region. Shorter PRT was found for the flow patterns with the highest PI, as compared to the runs with higher Reynolds/Womersley numbers and lower PI ratios. We revealed strong anti-correlation between PI and PRT, i.e. if a given flow pattern is characterized by a high pulsatility index, the measured particle residence time is expected to be low. Correlations between PRT and other WSS related properties are not as obvious, yet the trends of decreasing values with increasing PRT are clearly seen. Further study is needed, since it seems likely that quantitative correlation between PRT and WSS related properties could be established given a larger data base and a higher quality measurements in the near wall region.

To summarize, the dimensional, empirical and computational analysis of WSS related quantities demonstrate that the use of a single Reynolds number together with the Womersley number is not sufficient to characterize the pulsating flows with total flow reverse. In the present study, a pulsatility index that takes into account the amplitudes of the forward to reverse flow phases was utilized. We realize that in some case of the pulsatile flows, the definition of PI should be

extended in order to include the time intervals of forward/reverse flow phases. In a view of a possible *in-vivo* estimate of the particle residence time, which is shown here to be strongly correlated with the WSS properties of interest, an additional research in this direction can be important.

Acknowledgements The authors are thankful to Roman Povolotsky for the technical support and design of the experimental apparatus. This study was supported in part by a grant from the Nicholas and Elizabeth Slezak Super Center for Cardiac Research and Biomedical Engineering at Tel Aviv University and partially by the Israel Science Foundation, under Grant no. 782/08.

5 Conflict of Interest statement

We wish to confirm that there are no known conflicts of interest associated with this publication and there has been no significant financial support for this work that could have influenced its outcome.

References

1. Cheng, C. P., D. Parker, and C. A. Taylor. Quantification of Wall Shear Stress in Large Blood Vessels Using Lagrangian Interpolation Functions with Cine Phase-Contrast Magnetic Resonance Imaging. *Ann. Biomed. Eng.*, 30(8):1020–1032, 2002.
2. Evans, D.H., W.W. Barrie, M.J. Asher, S. Bentley, and P.R. Bell. The relationship between ultrasonic pulsatility index and proximal arterial stenosis in a canine model. *Circul. Res.*, 46:470–475, 1980.
3. Finol, E. A. and C. H. Amon. Flow-induced wall shear stress in abdominal aortic aneurysms: Part II—pulsatile flow hemodynamics. *Comput. Method. Biomec.*, 5(4): 319–28, 2002.

4. Gonzales, J. U., B. C. Thompson, J. R. Thistlethwaite, and B. W. Scheuermann. Role of retrograde flow in the shear stimulus associated with exercise blood flow. *Clin. Physiol. Funct.*, 28(5):318–325, 2008.
5. Gosling, R. G. and D. H. King. Arterial assessment by doppler-shift ultrasound. *Proc. R. Soc. Med.*, 67:447–9, 1974.
6. Gülan, U., B. Lüthi, M. Holzner, A. Liberzon, A. Tsinober and W. Kinzelbach. Experimental study of aortic flow in the ascending aorta via Particle Tracking Velocimetry. *Exp. Fluids*, 53(5): 1469–1485, 2012.
7. Haddad, K., O. Ertun, M. Mishra, and A. Delgado. Pulsating laminar fully developed channel and pipe flows. *Phys. Rev. E*, 81(1):16303, 2010.
8. Kertzscher, U., P. Debaene, L. Goubergrits, and K. Affeld. Experimental Assessment of Wall Shear Flow. In *Blood Flow Modeling and Diagnostics*, pages 109–134, 2005.
9. Kreizer, M. and A. Liberzon. Three-dimensional particle tracking method using FPGA-based real-time image processing and four-view image splitter. *Exp. Fluids*, 50(3):613–620, 2011.
10. Leguy, C. A. D., E. M. H. Bosboom, A. P. G. Hoeks, and F. N. Van de Vosse. Model-based assessment of dynamic arterial blood volume flow from ultrasound measurements. *Med. Biol. Eng. Comput.*, 47(6):641–8, 2009.
11. Malik, N. A. and T. H. Dracos. Particle tracking velocimetry in three-dimensional flows. *Exp. Fluids*, 15:279–294, 1993.
12. Nicholls, S. C., T. C. Koutlas, and D. E. Strandness. Clinical significance of retrograde flow in the vertebral artery. *Ann. Vasc. Surg.*, 5(4):331–6, 1991.
13. Pedley, T. J. *The Fluid Mechanics of Large Blood Vessels*. Cambridge University Press, 1980.
14. Reneman, R. S., T. Arts, and A. P. G. Hoeks. Wall shear stress—an important determinant of endothelial cell function and structure—in the arterial system in vivo. Discrepancies with theory. *J. Vasc. Res.*, 43(3):251–69, January 2006.
15. Sturgeon, V. *Experimental studies of pulsatile flows through compliant tubes undergoing forced wall motion: Applications to hemodynamics and stability*. Ph.D. thesis, University of California, Berkley, Berkley, USA, 2007.

-
16. Taylor, Z. J., R. Gurka, G. A. Kopp, and A. Liberzon. Long-Duration Time-Resolved PIV to Study Unsteady Aerodynamics. *IEEE Trans. Instr. Meas.*, 59(12):3262–3269, 2010.
 17. Thompson, R. S., B. J. Trudinger, and C. M. Cook. Doppler ultrasound waveform indices: A/B ratio, pulsatility index and Pourcelot ratio. *Br. J. Obstet. Gynaecol.*, 95(6):581–588, 1988.
 18. Uchida, S. The pulsating viscous flow superposed on the steady laminar motion of incompressible fluid in a circular pipe. *J. Fluid Mech.*, 1956.
 19. Womersley, J. R. Method for the calculation of velocity, rate of flow and viscous drag in arteries when the pressure gradient is known. *J. Physiol.*, 127(3):553, 1955.

List of Figures

1	Hydraulics system schematics: the flow is created by the controlled gear pumps and the reverse flow phase is due to the additional gear pump installed in the opposite flow direction. Voltage control of the pumps and the feedback from the flow meter and pressure transducers are regulated using the PC	17
2	Different types of generated flow patterns: (A) Unipolar sine with a secondary flow rate peak. (B) Dipolar sine. (C) Unipolar sine with total flow reversal.	18
3	Velocity measurement systems: (a) PIV setup scheme (b) 3D-PTV experimental setup.	19
4	DPIV measured velocity profiles (symbols) and the corresponding Womersley solution (lines) for 16 runs and different phases (color online).	20
5	Normalized WSS related quantities variation with frequency and pulsatility index. (a) Mean WSS. (b) WSS magnitude. (c) Oscillatory index. (d) WSS gradient. Values calculated from the simulation are presented by lines ($\alpha = 6$ - blue solid line, $\alpha = 9$ - red dashed line, $\alpha = 11$ - green dotted line and $\alpha = 13$ - black dash-dot-dash line) . Values calculated from direct measurements are presented with symbols, while triangular markers represent the sets with reverse flow phase.	21
6	Mean particle residence time (PRT) for the three representative runs as a function of the interrogation sphere radius, r_0	22
7	Particle residence time as a function of the following parameters: (a) pulsatility index (PI) (b) oscillatory shear index (OSI) (c) wall shear stress gradient (WSSG).	23

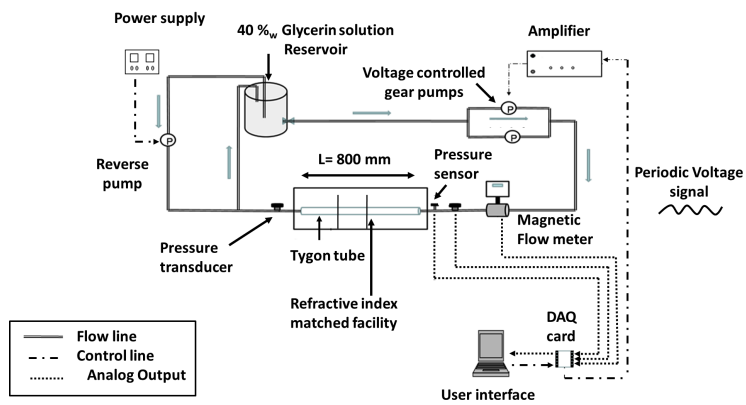


Fig. 1 Hydraulics system schematics: the flow is created by the controlled gear pumps and the reverse flow phase is due to the additional gear pump installed in the opposite flow direction. Voltage control of the pumps and the feedback from the flow meter and pressure transducers are regulated using the PC

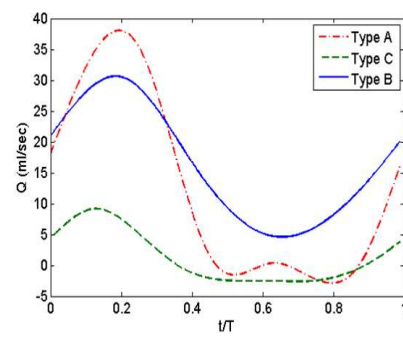


Fig. 2 Different types of generated flow patterns: (A) Unipolar sine with a secondary flow rate peak. (B) Dipolar sine. (C) Unipolar sine with total flow reversal.

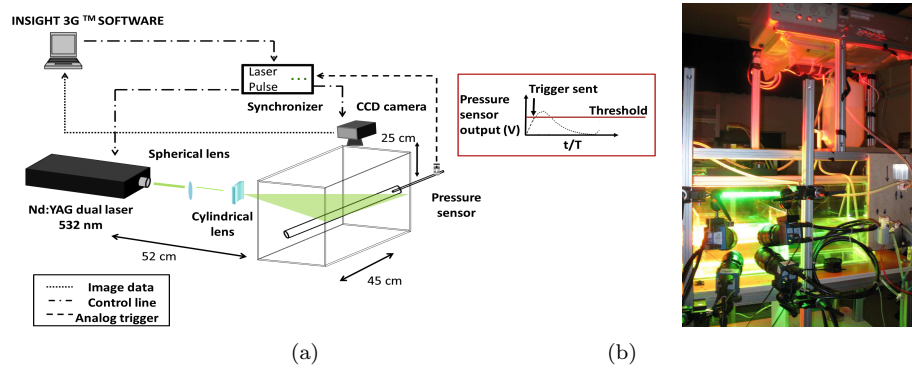


Fig. 3 Velocity measurement systems: (a) PIV setup scheme (b) 3D-PTV experimental setup.

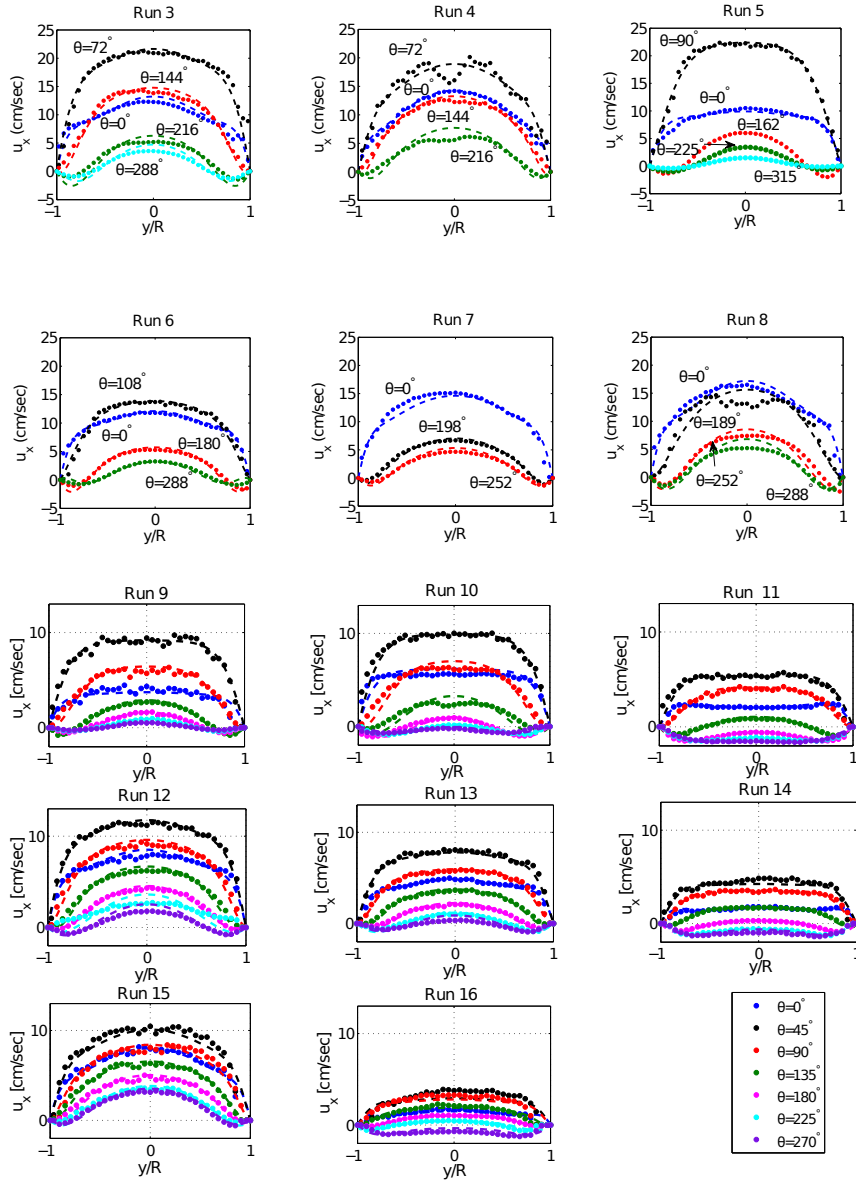


Fig. 4 DPIV measured velocity profiles (symbols) and the corresponding Womersley solution (lines) for 16 runs and different phases (color online).

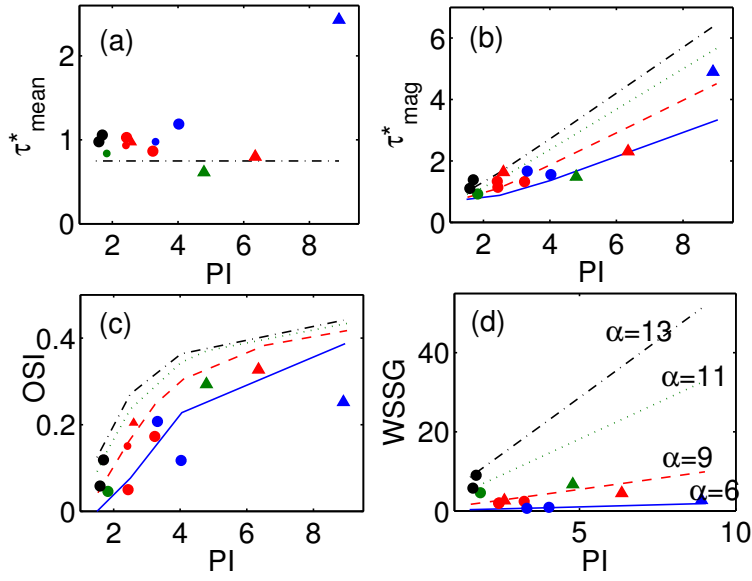


Fig. 5 Normalized WSS related quantities variation with frequency and pulsatility index. (a) Mean WSS. (b) WSS magnitude. (c) Oscillatory index. (d) WSS gradient. Values calculated from the simulation are presented by lines ($\alpha=6$ - blue solid line, $\alpha=9$ - red dashed line, $\alpha=11$ - green dotted line and $\alpha=13$ - black dash-dot-dash line). Values calculated from direct measurements are presented with symbols, while triangular markers represent the sets with reverse flow phase.

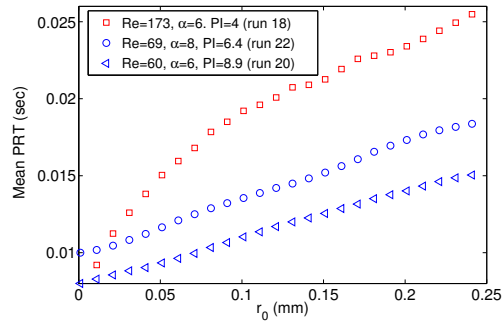


Fig. 6 Mean particle residence time (PRT) for the three representative runs as a function of the interrogation sphere radius, r_0 .

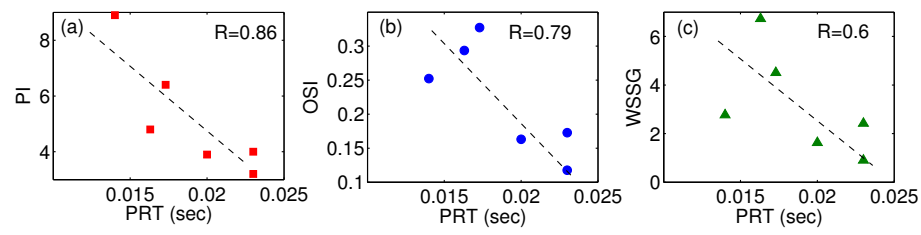


Fig. 7 Particle residence time as a function of the following parameters: (a) pulsatility index (PI) (b) oscillatory shear index (OSI) (c) wall shear stress gradient (WSSG).

List of Tables

- 1 Summary of experimental runs for the various wave forms (unipolar, bipolar sine, square wave), periods, Re_{\max} , α and PI. Runs 1 and 2 were performed at steady flow rate for the calibration purposes and are not shown here. 25

Run	Waveform	T (sec)	Re_{max}	α	PI	Method
3	Dipolar sine	2	788	9	2.4	PIV
4	Unipolar sine	1	806	13	1.6	PIV
5	Unipolar sine	4	607	6	3.3	PIV
6	Unipolar sine	2	540	9	2.6	PIV
7	Square wave	1	630	13	1.7	PIV
8	unipolar sine	2	942	9	1.5	PIV
9	unipolar sine	4	173	6	4	PIV, 3D-PTV
10	unipolar sine	4	213	6	3.9	PIV, 3D-PTV
11	unipolar sine	4	60	6	8.9	PIV, 3D-PTV
12	unipolar sine	2	353	8	2.4	PIV
13	unipolar sine	2	192	8	3.2	PIV,3D-PTV
14	unipolar sine	2	69	8	6.4	PIV, 3D-PTV
15	unipolar sine	1.2	336	11	1.8	PIV
16	unipolar sine	1.2	64	11	4.8	PIV,3D-PTV

Table 1 Summary of experimental runs for the various wave forms (unipolar, bipolar sine, square wave), periods, Re_{max} , α and PI. Runs 1 and 2 were performed at steady flow rate for the calibration purposes and are not shown here.